Original Article

Institution of MECHANICAL ENGINEERS
Journal of AEROSPACE ENGINEERING

Proc IMechE Part G:
J Aerospace Engineering
2018, Vol. 232(10) 1887–1902

DOI: 10.1177/0954410017704217
journals.sagepub.com/home/pig
SAGE

Optimal design and experiment of propellers for high altitude airship

Jun Jiao, Bi-Feng Song, Yu-Gang Zhang and Yu-Bin Li

Abstract

The multi-objective optimization design method and experimental validation of the propeller for high altitude airships are presented in this paper. The method of predicting the propeller's aerodynamic characteristics is based on the vortex theory. The non-dominated sorting genetic algorithm II is introduced and applied to solve the optimization problem. Then the optimization model which aims to design an efficient and lightweight propeller for high altitude airships is established based on the conditions of high altitude airships propulsion system. In addition, the effects of various design variables including pitch angle, chord length, diameter, rotational speed, and the number of blades on high altitude propeller performance are presented and discussed in a gradual manner. The optimization results indicate that the desirable tradeoff between the efficiency and weight of high altitude propeller is associated with the absorbed power, structural strength, and even the manufacturing and installation conditions. In order to evaluate the mathematical model and performance of the optimized propeller, wind tunnel experiments of scaled model on the basis of scaling laws and the full-scale propeller test using mobile testing system were carried out. It is shown that results obtained from the experiments agree well with those of the numerical calculation, which verifies that the designed propeller can satisfy the requirements of the high altitude airships' propulsion system.

Keywords

Propeller, high altitude airship, optimization design, vortex theory, NSGA-II, wind tunnel experiment, scaling law, testing system

Date received: 4 April 2016; accepted: 20 March 2017

Introduction

The potential of lighter-than-air (LTA) platforms for high altitude application has attracted growing interest in the past few decades.[1] In particular, high altitude airships (HAA) is considered as an excellent platform for many different purposes in both civil and military fields such as aerial exploration, communications support, Intelligence, Surveillance, and Reconnaissance (ISR).[2,3] The concept of an HAA began with the United States Navy in the late 1970s when the initial program was sponsored by Navy and developed in the 1980s. Since then, along with the rapid progress of aerospace technologies,[4] there have been numerous researches and trials focusing on the issues of designing the HAA to achieve a great performance, such as High-Altitude Airship of Lockheed Martin Company,[5] Stratospheric Platform Airship of Japan,[6] Stratospheric Airship Program of South Korea,[7] "Berkut" Solar Powered Airship in Russia,[8] and Multibody Advanced Airship for Transport Project of European Union.[9]

With the development of airships, the propeller driven by an electric motor is widely used in the propulsion system of HAA, which allows much more control over the craft and changes in mission goals.[8,10] In order to make full use of the power of engine or electromotor and reduce the energy consumption, the propeller system needs improving its efficiency and reducing weight as much as possible to satisfy HAA's requirements during the high altitude and long endurance flight period. Thus, it is essential to establish a reliable numerical method to predict the high altitude propeller's propulsive performance and weight. In reality, the design of the propeller based on minimum induced losses started with Betz and Goldstein at the beginning of the 20th century and then was developed by a variety of excellent scientists for more than a century.[11] These

School of Aeronautics, Northwestern Polytechnical University, Xi'an, China

Corresponding author:
Jun Jiao, School of Aeronautics, Northwestern Polytechnical University, Xi'an 710072, China.
Email: jiao34554@hotmail.com

numerical methods are still utilized in the design of high altitude propellers, and also play a significant role in the preliminary design of HAA propulsion system.[12–14]

In addition, HAA is a kind of low-dynamic vehicles cruising in the stratosphere where its atmospheric density is extremely low, resulting in a low Reynolds number of the high altitude propeller. Therefore, the similarity criterion of the scale-propeller for the wind tunnel experiment should be confirmed to simulate the real flight conditions.[15] And it is also significant to evaluate the aerodynamic characteristics of the full-scale propeller for the purpose of validation. Several approaches of propeller testing such as wind tunnel experiment, APEX Flight Experiment and atmospheric Drop Test are proposed and conducted in the past and deserve being researched continually.[12,16]

In this study, a method of predicting the aerodynamic performance and weight is integrated into the multi-objective optimization design of a high altitude propeller. Based on the vortex theory and the non-dominated sorting genetic algorithm II (NSGA-II) algorithm, an investigation of the design variables, including pitch angle, chord length, diameter, rotational speed and the number of blades on high altitude propeller performance and weight is discussed in detail. Meanwhile, according to the wind tunnel experiment of scaled propeller model and the full-scale propeller test on a mobile testing system, the performance of the designed propeller are obtained comprehensively and proved to meet the requirements of the HAA's propulsion system.

The remainder of this paper is organized as follows. The upcoming section outlines the vortex theory of propeller as well as its implementation process. Next, the NSGA-II is briefly introduced to solve the multi-objective problem firstly. Afterwards, the optimization model of the high altitude propeller is built based on the design constraints of HAA's propulsion system. The scaling laws of the high altitude propeller in the wind tunnel are discussed, and the mobile testing system for full-scale propeller test is established. Subsequently, the numerical solutions of the optimization problem are conducted in a gradual manner, and the optimization results are discussed. Finally, the performance of the designed high altitude propeller is verified through the comparisons of experimental results and numerical calculations.

Propeller blade theory

Vortex theory

In order to design a propeller or to predict the performance of a rotating propeller accurately, various methods have been proposed to analyze the aerodynamic characteristics of the blade in detail. All of these methods involve the use of ''blade elements'', which subdivide the propeller into individual section along the radius. Each of these sections can be viewed as a two-dimensional airfoil section and analyzed individually when the associated parameters are confirmed. The forces acting on each section are finally integrated to obtain the thrust and torque of the overall propeller.[17]

Referring to Figure 1, the propeller is rotating with a rotational speed of n_s and advancing through the air with a velocity of V. The pitch angle, β, is defined relative to the zero lift line of the airfoil section, which varies with the radial distance r. Similar to finite wing theory, the total down wash angle, θ, is the sum of two parts, the advanced angle, φ, and the induced angle of attack resulting from the induced velocity ω, α_i, the contribution of one-blade element to the

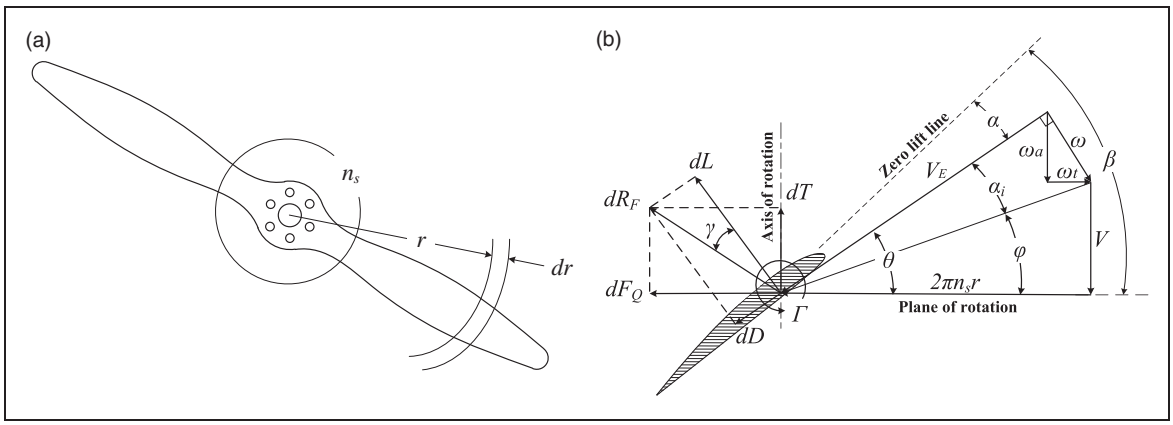

Figure 1. Section forces and velocities acting on a rotating propeller blade. (a) Front view of the propeller; (b) blade element at radius r. The blade is rotating with a speed of $2\pi n_s r$, V is the wind speed, β is the pitch angle, α is the angle of attack, θ is the down wash angle, which composed of the advanced angle, φ, and the induced angle of attack, α_i. The induced velocity, ω, is the sum the tangential and axial component of induced velocity, ω_t and ω_a. V_E is the total relative velocity of the airfoil section. The total force, dR_F, can be divided into the thrust, dT, and tangential force, dF_Q, or the differential lift and drag forces, dL and dD.

thrust, dT, and torque, dQ, are related to the differential lift and drag forces, and can be calculated by

$$dT = dL\cos(\theta) - dD\sin(\theta) = \tfrac{1}{2}\rho V_E^2 c[C_l\cos(\varphi+\alpha_i) - C_d\sin(\varphi+\alpha_i)]dr \quad (1)$$

$$dQ = r dF_Q = r[dL\sin(\theta) + dD\cos(\theta)] = \tfrac{1}{2}\rho V_E^2 c[C_l\sin(\varphi+\alpha_i) + C_d\cos(\varphi+\alpha_i)]r dr \quad (2)$$

The section lift and drag coefficient, C_l and C_d, depend on the local Reynolds and Mach number, Re and Ma, and aerodynamic angle of attack for the blade element, α. From the tangential and axial component of induced velocity, ω_t and ω_a, the angle of attack α can be determined as

$$\alpha = \beta - \varphi - \alpha_i = \beta - \theta = \beta - \tan^{-1}\left(\frac{V+\omega_a}{2\pi n_s r - \omega_t}\right) \quad (3)$$

And the induced angle can also be determined easily from the same geometry as

$$\alpha_i = \theta - \varphi = \tan^{-1}\left(\frac{V+\omega_a}{2\pi n_s r - \omega_t}\right) - \tan^{-1}\left(\frac{V}{2\pi n_s r}\right) \quad (4)$$

The total relative velocity, V_E, at the plane of the blade section is given by

$$V_E = \sqrt{(V+\omega_a)^2 + (2\pi n_s r - \omega_t)^2} \quad (5)$$

The Kutta–Joukowski theorem states that the lift on a finite propeller blade is related to the bound vorticity through the vortex lifting law. Thus, the local section circulation, Γ, of a propeller blade can be expressed as

$$\Gamma = \tfrac{1}{2} c C_l V_E \quad (6)$$

According to Goldstein's vortex theory, the induced velocity can be predicted under two hypotheses which also satisfy the Betz condition. First, the vortex sheet trailing from a rotating propeller blade was assumed to lie along a helical surface of the constant pitch. Second, the induced velocity was assumed to be normal to the resultant velocity. So the two parts of the induced velocity are related by

$$\frac{V+\omega_a}{2\pi n_s r - \omega_t} = \frac{\omega_t}{\omega_a} \quad (7)$$

This equation can be solved for ω_a as a function of ω_t

$$\omega_a = \tfrac{1}{2}\left[-V + \sqrt{V^2 + 4\omega_t(\omega r - \omega_t)}\right] \quad (8)$$

Goldstein's vortex theory relates the local tangential component of induced velocity, ω_t, to the bound circulation, Γ, around any blade section by

$$B\Gamma = 4\pi r\kappa\omega_t \simeq 4\pi r F\omega_t \quad (9)$$

The Goldstein's kappa factor, κ, is available in graphical form but never been presented in closed form. A close approximation of κ is known as *Prandtl's tip loss factor*, F, which can be expressed as

$$F = \frac{2}{\pi}\cos^{-1}\left\{\exp\left[-\frac{B(1-2r/d)}{2\sin\beta_t}\right]\right\} \quad (10)$$

where d is the propeller diameter, B is the number of blades, and β_t is the pitch angle at the propeller blade tip.

Calculation procedure

In the calculation process, one of the most difficult issues for vortex theory is to determine the induced velocity and angle, ω and α_i. The propeller blade geometry and operating conditions include the chord length, c, the pitch angle, β, the diameter of the propeller, d, the airfoil types, Y, of each section, the free stream wind speed, V, the rotor rotational speed, n_s, the number of blades, B, and the operating altitude, H. These parameters and their relationships associated with the lift and drag coefficients of each blade element is shown in Figure 2 in terms of the propeller blade theory. From the diagram, it is evident that the performance of the airfoil with a certain angle of attack, α, is mainly related to Reynolds and Mach numbers. Drela's XFOIL uses a linear-vorticity panel method for inviscid analysis as well as adopting an integral boundary-layer method for viscous analysis.[18] The XFOIL has proven to be a powerful and useful tool for the design and the analysis of the airfoil aerodynamic characteristics at low-speed and low Reynolds numbers.[19] So in the design process, XFOIL (version 6.99) is employed for the calculation of C_l and C_d of the airfoils along the blade radius with

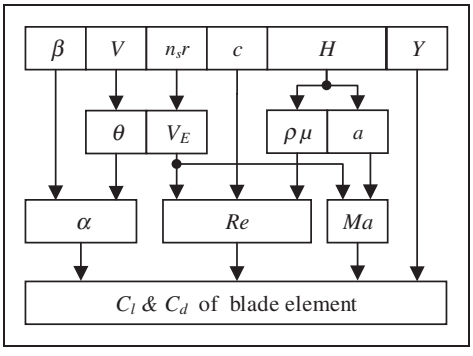

Figure 2. Relationship of the parameters associated with blade element aerodynamics.

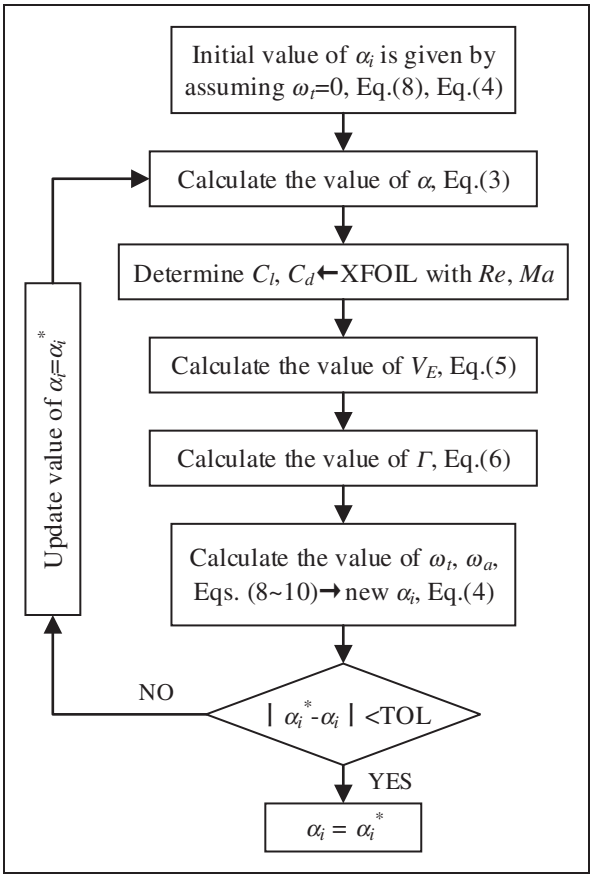

Figure 3. Calculation flowchart for the induced angle and velocity.

different angle of attack, Reynolds and Mach numbers.

After achieving the local lift and drag coefficients of the blade section, an iterative approach of the induced angle, α_i, proceeds as outlined in Figure 3. The induced velocity, ω, and its tangential and axial components, ω_t and ω_a could also be calculated during the iteration, then the differential thrust and torque, dT and dQ of each section are uniquely determined.

The thrust and torque on the overall propeller can be calculated by integrating the differential quantities from the hub diameter, r_h, to the tip diameter, r_t, using the following equations

$$T = \int_{r=r_h}^{r_t} dT \tag{11}$$

$$Q = \int_{r=r_h}^{r_t} dQ \tag{12}$$

Optimal design of high altitude propeller

Multi-objective optimization theory

Multi-objective optimization problem involves minimizing or maximizing multiple objective functions subject to a set of constraints, and it is an extension of the single objective optimization problem.[21] A general multi-objective optimization design can be described as

$$\begin{aligned} \text{Min/Max} \quad & F(\mathbf{x}) = (f_1(\mathbf{x}), \ldots f_k(\mathbf{x})) \\ \text{Subject to :} \quad & g_i(\mathbf{x}) \leqslant 0,\ i = \{1, \ldots, m\}, \\ & h_j(\mathbf{x}) = 0,\ j = \{1, \ldots, p\}, \end{aligned}$$

where $F(\mathbf{x})$ is the vector-valued function, and $\mathbf{x}$ is a n-dimensional decision variable vector $\mathbf{x} = (x_1, \ldots, x_n)$ from some universe Ω, $g_i(\mathbf{x}) \leqslant 0$ and $h_j(\mathbf{x}) = 0$ represent constraints.

The concept of Pareto optimality is integral to the theory and the solving of MOPs. For a given MOP, a vector $\mathbf{u} = (u_1, \ldots, u_k)$ is said to dominate another vector $\mathbf{v} = (v_1, \ldots, v_k)$ (denoted by $\mathbf{u} \leqslant \mathbf{v}$) if and only if $\mathbf{u}$ is partially less than $\mathbf{v}$, and that is

$$\text{iff } \forall i \in \{1, \ldots k\}, u_i \leqslant v_i \text{ and } \exists i \in \{1, \ldots k\} : u_i < v_i$$

The Pareto optimal set, P^*, and the Pareto Front, PF^*, is defined as

$$\begin{aligned} P^* &= \{x \in \Omega | \neg \exists x' \in \Omega \quad F(x') \leqslant F(x)\} \\ PF^* &= \{u = F(x) | x \in P^*\} \end{aligned}$$

The NSGA-II, which is an improved version of NSGA, is one of the contemporary multi-objective evolutionary algorithms that exhibits high performance and has been widely applied in various disciplines. The algorithm makes use of a fast nondominating sorting approach to discriminate solutions, which is based on the concept of Pareto dominance and optimality.[21]

The flow chart of the NSGA II program is shown in Figure 4. It starts with a random initial generation. First, the parents and offspring are combined. When the objective functions of all strings in a generation are calculated, the solutions are classified into various nondominated fronts. The crowded tournament selection operator is used to compare two solutions and returns the winner of the tournament according to two attributes: (1) a nondominated front in the population and (2) a local large crowding distance. The first condition makes sure that the chosen solution lies on a better non-dominated front, and the second condition ensures a better spread among the solutions. The simulated binary crossover (SBX) is used here to create two offspring from two-parent solutions. The random simplest mutation operator is applied randomly to create a solution from the entire search space.[22]

Optimization model and scheme

Objective function. The ability of airships to operate for an extended duration of time (months to years) at

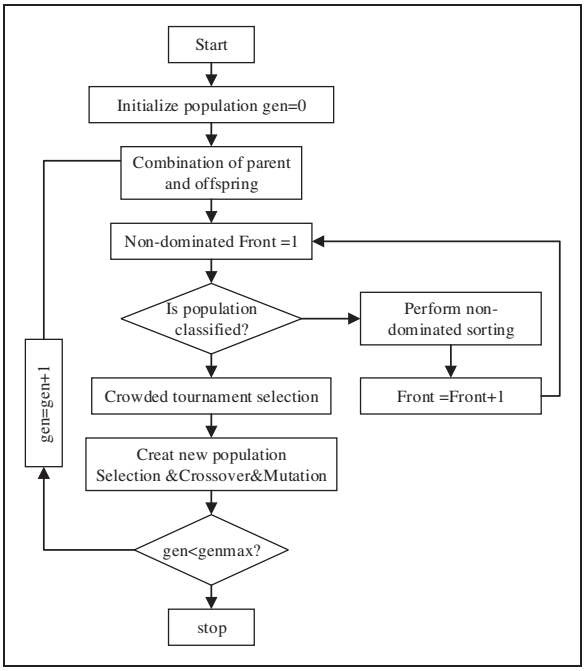

Figure 4. Flow chart of NSGA-II optimization procedure.

high altitudes requires a renewable based power system with an efficient propulsion system. Therefore, in order to take full advantage of the motor power and reduce energy consumption, the propeller systems of HAA need to be highly efficient and lightweight. So, one of the objectives is the aerodynamic efficiency of the propeller at the design point. Besides, the propeller's weight also directly affects the total weight of the power system and needs to be considered during the design process. In general, high altitude propeller is made of composite materials. The blade density distribution varies greatly because of the different lamination design and the complex shape. It is very hard to obtain the blade weight by using composite laminate theory. Therefore, weight estimation of the propeller can be converted into blade surface area calculation if the layer thickness and material density are considered to be the same. It is an effective approach to avoid building complex structure model of the composite blade. The two objectives are defined in the following equation

$$Objectives: \quad f_1(x) = \max(\eta), \quad f_2(x) = \min(S) \tag{13}$$

The aerodynamic efficiency of the propeller is defined as the propulsive power, P_p, divided by the brake power, P, which will be calculated based on the vortex theory. λ is the advance ratio of a propeller, which is defined as $\lambda = V/n_s d$.

$$\eta = \frac{P_p}{P} = \frac{TV}{Q2\pi n_s R} = \frac{C_T \lambda}{C_P} \tag{14}$$

As shown in Figure 5, the blade area is obtained by numerical spanwise integration of the length for each blade section profile, which can be expressed as

$$S = B \lim_{dr \to 0} \sum \Delta S = B \int_{r=r_h}^{r_t} l(x, y) \mathrm{d}r \tag{15}$$

where $l(x, y)$ is the length equation of the blade profile, (x_{i0}, y_{i0}) the airfoil coordinates of a unit chord, (x_i, y_i) the transformed airfoil coordinate of the propeller blade.

The length of the blade profile is defined as the limit of the lengths of the inscribed polygons with vertices

$$l(x, y) = \sum_{i=1}^{m} \sqrt{(x_{i+1} - x_i)^2 + (y_{i+1} - y_i)^2}, \quad \times \begin{cases} x_i = c(x_{i0} \cos\beta + y_{i0} \sin\beta) \\ y_i = c(y_{i0} \cos\beta - x_{i0} \sin\beta) \end{cases} \tag{16}$$

Thus, after applying equations (15) and (16), the blade surface area of the whole propeller can be obtained.

Design variables and constraints. The propeller blade geometry and operating conditions determine the aerodynamic efficiency of the propeller. The high-lift airfoil series self-developed are used in this case, and the position of these airfoils is also previously determined. The relative thickness of the blade airfoil arrangement decreases monotonically from the blade root to the tip. The airfoils of typical profiles across the blade and their performance are presented in Figures 6 and 7.

In addition to the cross-sectional airfoil, the geometry of the propeller blade is mainly determined by the distribution of chord and pitch angle. In order to make the blade shape smooth and continuous along the spanwise direction, the cubic Bézier curve is used to describe the blade chord and the pitch angle distribution

$$c(x) = (1-x)^3 c_0 + 3x(1-x)^2 c_1 + 3x^2(1-x)c_2 + x^3 c_3 \tag{17}$$

$$\beta(y) = (1-y)^3 \beta_0 + 3y(1-y)^2 \beta_1 + 3y^2(1-y)\beta_2 + y^3 \beta_3 \tag{18}$$

where c_0, c_1, c_2, and c_3 represent four control points of the chord distribution, one at hub, one at tip and two at intermediate stations, β_0, β_1, β_2, and β_3 represents the control points of the pitch angel distribution, x, y changes in [0, 1], the range of eight parameters is limited as follows

$$c_{i\min} \leqslant c_i \leqslant c_{i\max} \quad \beta_{i\min} \leqslant \beta_i \leqslant \beta_{i\max} \quad \mathrm{i} = 0, \ldots, 3$$

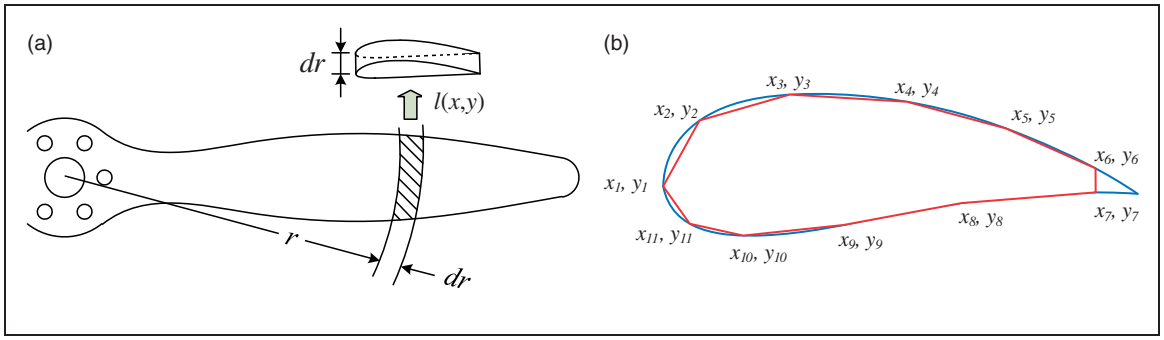

Figure 5. Method of estimating the blade surface area: (a) integration along the propeller blade; (b) arc length of blade section.

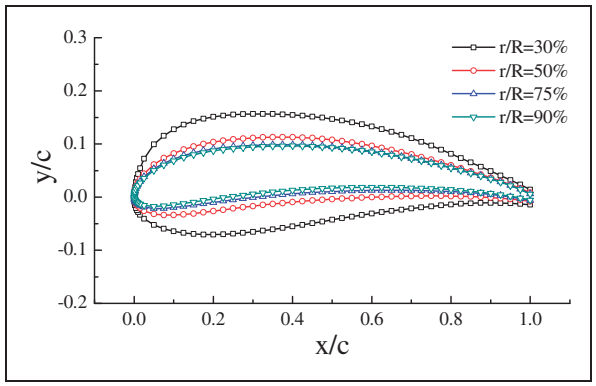

Figure 6. Airfoil geometries of several sections across the blade.

Aside from the geometry (airfoil and blade twist) of the propeller blade, the propeller's diameter and the number of blades are important factors which will significantly affect the performance of the propeller at a given altitude. In addition, in order to take into account the performance of the drive motor, the range of values for rotational speed should be subject to a reasonable limitation as a design variable. Thus, the design variables and their bounds are described in Table 1.

$$\textit{Design variables}: \quad c_0, c_1, c_2, c_3, \beta_0, \beta_1, \beta_2, \beta_3, \mathrm{d}, n_s, B \tag{19}$$

Besides the geometrical dimension constraint, several important constraints are applied here to satisfy the performance of the propeller for HAA. The required thrust under the flight condition and the rated power absorbed from the motor are both restricted based on the task requirement and propulsion system of HAA. Because the diameter and the rotational speed are both changing during the design process, the tip Mach number defined in equation (20) of the propeller must be limited around 0.7 Mach, which can be achieved easily under high altitude and low density environment.[23] This is done to avoid the formation of shock waves over the surface of the blade, which can severely reduce its performance if not destroy the propeller.

$$Ma_{tip} = \frac{\sqrt{V^2 + (\pi n_s d)^2}}{a} \tag{20}$$

$$\textit{Constraints}: \quad T \geqslant T_{\min}, \; P_b = P_{rated}, \; Ma_{tip} \leqslant Ma_{\max} \tag{21}$$

The equality and inequality constraints according to the requirements of the HAA propulsion system are summarized in Table 2.

Design process. It is noted that there are many design variables during the propeller optimization design, apart from the change of blade twist and chord, the complexity further increases due to the variation of the diameter and the number of the propeller blades. In general, the reason multi-blade propellers seem to be inefficient is the need to use considerable lower diameter propellers (in comparison to two-blades) in the propeller design process, but the situation is quite different in the high altitude propeller design. The restrictions on the size of the high altitude propeller are not as strict as those of the conventional aircraft. In addition, the engine power of the HAA propulsion system is usually relatively large, the airship designer needs to design a propeller capable of efficiently absorbing that higher power at high altitude. Increasing the diameter or the number of blades can both be helpful to transfer more power produced by the engine to the air. But obviously, these changes will have different effects on the efficiency and weight of the propellers.

Therefore, in order to obtain the effect of the different design variables during the optimization of high altitude propeller, the design process will be carried out in a gradual manner. Initially, the two-bladed propellers with fixed diameter will be considered, and the diameter of the propellers will be changed to understand its effect on the two contrary goals. At last, the influence of the number of blades on the optimization design will be investigated subsequently under the same design constraints.

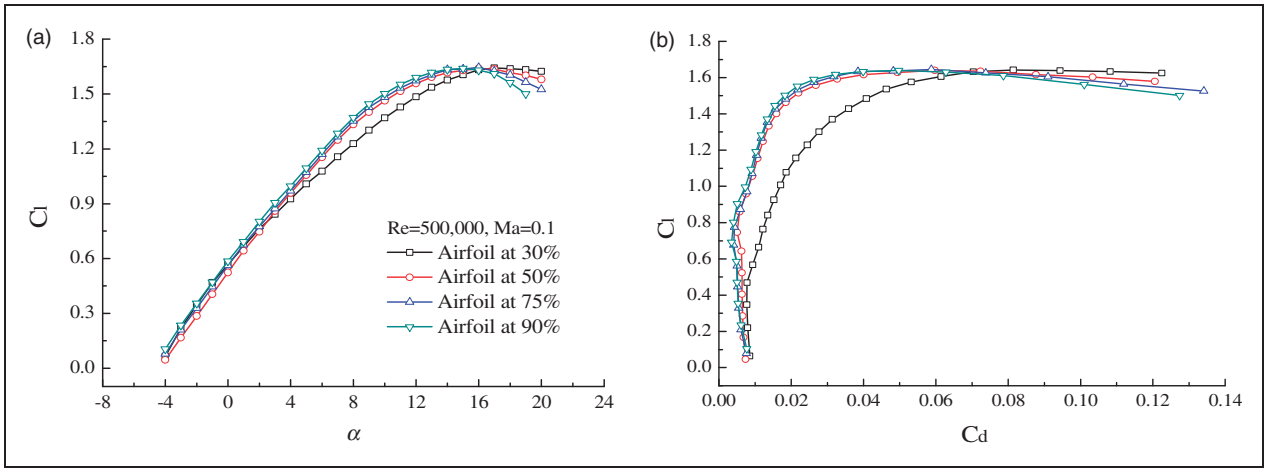

Figure 7. Airfoil performance in XFOIL for $Re = 5.00 \times 10^5$ and $Ma = 0.1$: (a) C_l vs α; (b) C_l vs C_d.

Table 1. Design variables and their ranges.

Design variable	Description	Range
C_0	The control parameters of chord distribution, m	0.1–0.6
C_1		0.2–1.0
C_2		0.2–1.0
C_3		0.1–0.6
β_0	The control parameters of pitch angle distribution, degree	20–60
β_1		20–60
β_2		1–30
β_3		1–30
d	Propeller's diameter, m	6.2, 6.8, 7.4
n_s	Propeller's rotational speed, rpm	500–600
B	Number of blades	2, 3, 4

Table 2. Design constraints.

Constraint	Description	Value
H	Flight altitude	20 km
V	Wind velocity	20 m/s
T	Thrust of propeller	$\geqslant$900 N
P	Propeller absorbed power	25.5 kW
Ma_{tip}	Mach number of the blade tip	$\leqslant$0.7

Experimental setup

Wind tunnel experiment

The wind tunnel test of the scaled model needs to follow the similitude to ensure valid results, which consist of geometric, kinematics, and dynamic similarity. When the geometric and kinematics similarity are confirmed, the main parameters affecting dynamic similarity are the Reynolds number and the Mach number. However, the low Reynolds number effect has the greater impact on the aerodynamics of the high altitude propeller. Therefore, the main similarity criteria required here are the advance ratio and Reynolds number, which are expressed as follows[15]

$$\begin{cases} (Re)_{\text{model}} = (Re)_{\text{prototype}} = \left(\frac{\rho V c}{\mu}\right)_{\text{model}} = \left(\frac{\rho V c}{\mu}\right)_{\text{prototype}} \\ (\lambda)_{\text{model}} = (\lambda)_{\text{prototype}} = \left(\frac{V}{n_s d}\right)_{\text{model}} = \left(\frac{V}{n_s d}\right)_{\text{prototype}} \end{cases} \tag{22}$$

Then the scaling laws between the prototype and model can be formulated in the following equation

$$\begin{aligned} d_r &= \frac{c_m}{c_p} = \frac{d_m}{d_p} \\ n_r &= \frac{n_{sm}}{n_{sp}} = \frac{\rho_p \mu_m d_p^2}{\rho_m \mu_p d_m^2} = \frac{\nu_r}{d_r^2} \\ V_r &= \frac{V_m}{V_p} = \frac{\rho_p \mu_m d_p}{\rho_m \mu_p d_m} = \frac{\nu_r}{d_r} \end{aligned} \tag{23}$$

where x_r is defined as the ratio of the associated parameters indicated by the subscript, ν is the kinematic viscosity, $\upsilon = \mu/\rho$, μ is the dynamic viscosity of the fluid, and ρ is the density of the fluid.

The nondimensional aerodynamic parameters of the scaled model are equal to those of prototype if the similarity principles are followed, and that is $C_{Tm}/C_{Tp} = C_{Qm}/C_{Qp} = C_{Pm}/C_{Pp} = 1$. The force measured from the model at that condition is then scaled to be expected for the real application

$$\begin{aligned} T_r &= \frac{T_m}{T_p} = \frac{\rho_m n_{sm}^2 d_m^2 C_{Tm}}{\rho_p n_{sp}^2 d_p^2 C_{Tp}} = \rho_r n_{sr}^2 d_r^4 = \rho_r \nu_r^2 \\ Q_r &= \frac{Q_m}{Q_p} = \frac{\rho_m n_{sm}^2 d_m^5 C_{Qm}}{\rho_p n_{sp}^2 d_p^5 C_{Qp}} = \rho_r n_{sr}^2 d_r^5 = \rho_r \nu_r^2 d_r \\ P_r &= \frac{P_m}{P_p} = \frac{\rho_m n_{sm}^2 d_m^5 C_{Pm}}{\rho_p n_{sp}^2 d_p^5 C_{Pp}} = \rho_r n_{sr}^3 d_r^5 = \frac{\rho_r \nu_r^3}{d_r} \end{aligned} \tag{24}$$

This wind tunnel test was conducted in the NF-3 low-speed wind tunnel at Northwestern Polytechnical University of China by following the Reynolds number similarity criteria and the advance ratio similarity criteria discussed above. The facility is a direct-circuit wind tunnel incorporating a $12\,m \times 3.5\,m \times 2.5\,m$ test section. The scaled propeller model is driven by a converter motor, and the experimental data is measured by a six component cassette strain gauge balance and other equipment, as shown in Figure 8.

Full-scale propeller test

The blade of the high altitude propeller is long enough to be seen as a kind of slender structure. So it is necessary to check the aerodynamic characteristics of the full-size propeller, which is prone to deform during the process of constant rotation. So a test apparatus whereby all experimental equipment and electronics are mounted on a mobile platform is designed and constructed.[24] This testing system allows full-size propeller experiment to be carried out at different attitudes under 4 km and offers significant time and cost benefits compared to other projects.

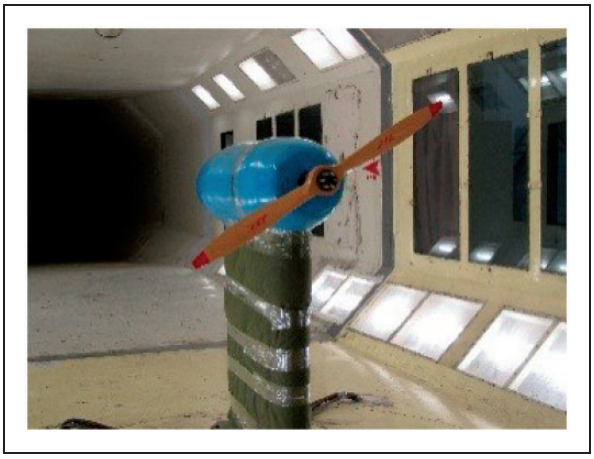

Figure 8. Wind tunnel test.

The configuration of a mobile testing system, shown in Figure 9, is composed of three parts. The test platform is used to install the propeller model and its driving device including the DC motor with speed reducer, the generators and stabilized voltage supply. In the measurement and control system, the force sensors are used to measure the aerodynamic force of the propeller, and the real-time data is collected by the NI Data acquisition system configured with NI cDAQ-9188 and several C Series I/O Modules including NI 9237, NI 9203, NI 9205, and NI 9401. By using an anemometer and a barometer, the airspeed and atmospheric pressure will be monitored and recorded by a control computer through USB to RS485 Converter Cables. The working parameters of the driving motor including start-stop, rotational speed, acceleration, and deceleration are also be regulated by the control computer through the motor controller. The test platform and control system are supported by the delivery platform which is a refitted vehicle and transported along a straight roadway to create the relative wind speed during the experiment. Schematic and physical diagrams of the mobile testing system are presented in Figure 10.

Results and discussion

Analysis of two-bladed propeller

The optimization results of the two-bladed propeller with 6.8-meter diameter are shown in Figure 11. The optimal region is divided into two parts by the Pareto frontier. Part I is an ideal solution region that cannot be reached under the design conditions, while part II

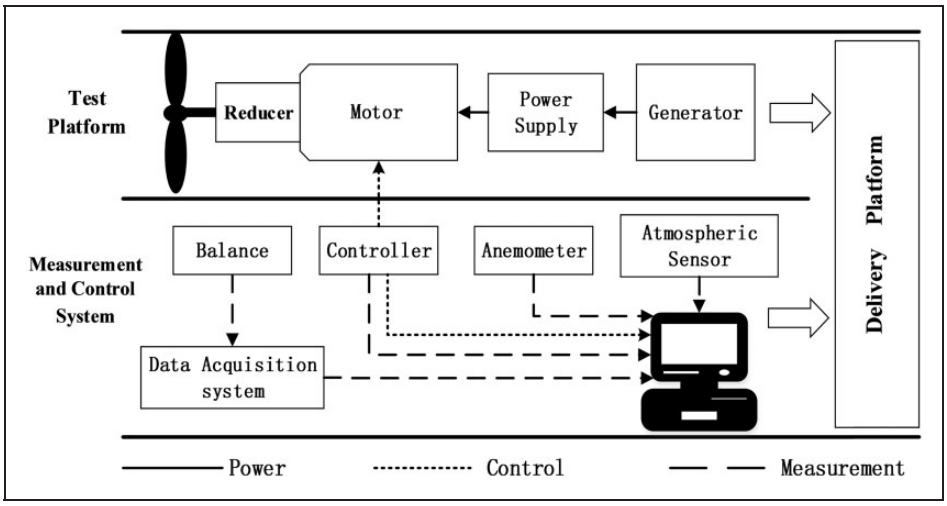

Figure 9. Configuration of the mobile testing system.

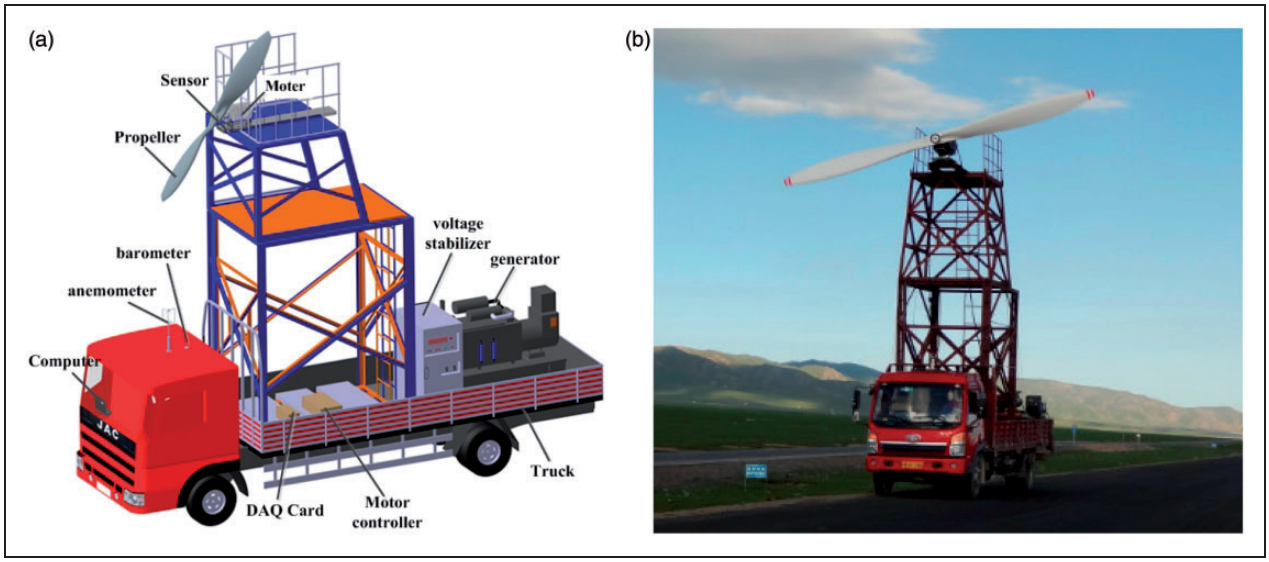

Figure 10. Full-scale propeller test system: (a) model in CATIA; (b) field test.

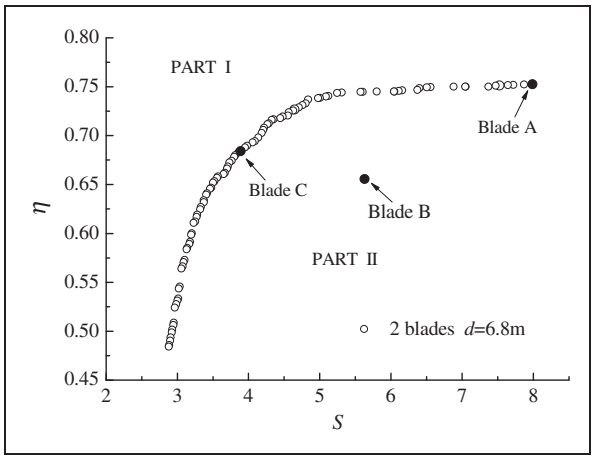

Figure 11. Pareto-optimal solution of a 6.8-meter propeller with two blades.

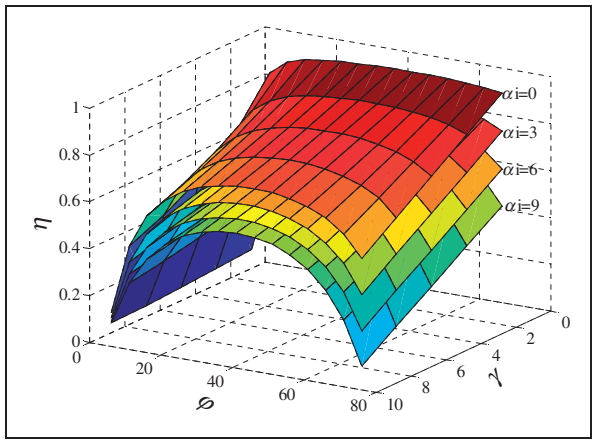

Figure 12. The relationship between the propeller blade element efficiency and advanced angle.

is a feasible solution region. The monotonicity of the Pareto frontier shows that the increase of the propeller efficiency is accompanied by the increase of the blade weight, indicating that the two design goals have a certain degree of conflict.

To explain the Pareto optimal solution set better, three blades marked in Figure 11 are further analyzed. Blade A is a highly efficient propeller under the power and thrust constraints, it has the most reasonable speed triangle distribution from the propeller root to tip. Blade B is a result in the feasible solution region, and the unreasonable distribution of the chord length and pitch angle lead to the relatively low efficiency compared with the blade on the Pareto Frontier under the same blade area conditions. On the other hand, although the efficiency of the blade C reduces by about 9% compared with blade A, the change of blade area shows a more significant decline of 47%.

To understand the physical phenomena behind the results, a preliminary analysis is presented here. It is known that propeller performance is largely determined by the efficiency of blade element,[25] which can be calculated by the following equation with reference to Figure 1 (the advanced angle, $\varphi = \arctan(V/2\pi n_s r)$, the drag-lift angle, $\gamma = \arctan(D/L)$ and α_i is the induced angle)

$$\eta_b = \frac{dP_p}{dP} = \frac{V}{2\pi n_s r}\frac{dT}{dQ} = \frac{\tan\varphi}{\tan(\varphi + \alpha_i + \gamma)} \tag{25}$$

For different theta values, the relationship between the propeller efficiency and the advanced angle is shown in Figure 12. The advanced angle with high-performance is around 30°–50° for each curve with a fixed induced angle and drag-lift angle. The efficiency of blade element decreases with the values of induced angle and drag-lift angle of the airfoil for the fixed

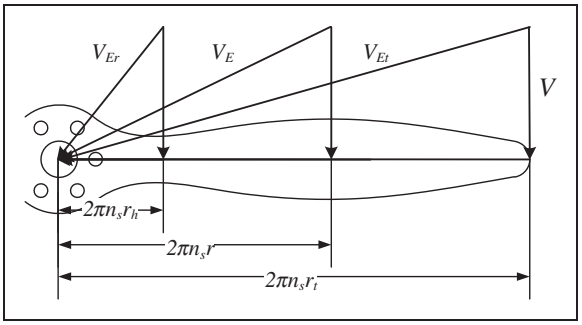

Figure 13. Speed triangle along the propeller blade.

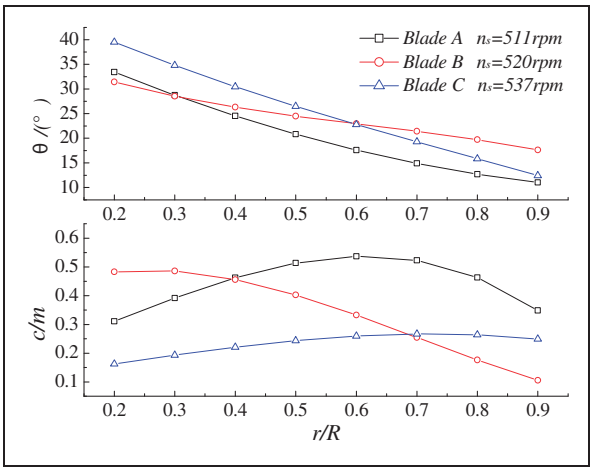

Figure 14. Chord and pitch angle distributions of blades A, B, and C.

advanced angles. When $\varphi > 15°$ and $\alpha_i + \gamma < 4°$, the efficiency is no less than 80%. However, the high altitude propeller cannot always meet these conditions from propeller's root to tip, because the rotational speed of each airfoil section is quite different as shown in Figure 13. So the propeller efficiency, as well as the weight, depend heavily on a reasonable distribution of the twist angle and chord length.

The geometries and operating speed of blades A, B, and C are shown in Figure 14. The speed triangle distribution of Blade A is more reasonable. Thus, it has the highest aerodynamic efficiency among the three blades. Besides that, it can be seen from the figure that some of the propeller efficiency need to be sacrificed to achieve the goal of light weight. But the reduction of chord length and the increase of pitch angle need to change by some disciplines to maintain the speed triangle at its highly efficient operation region. Moreover, the rotational speed of propeller with small blade area increases to meet the design constraints of the absorbed power and thrust.

Figure 15 presents the Pareto-optimal solutions of two-bladed propellers with different diameters. The propeller with large diameter mostly has a higher aerodynamic efficiency than the small one under the same condition of surface area. This is because the propeller blade can be regarded as the wing model

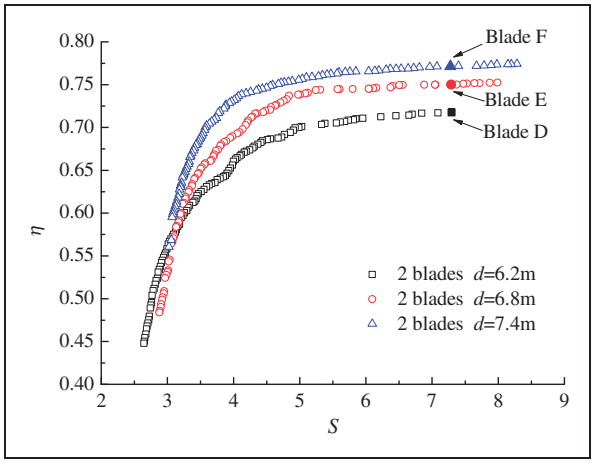

Figure 15. Pareto-optimal solutions of two-bladed propellers with different diameters.

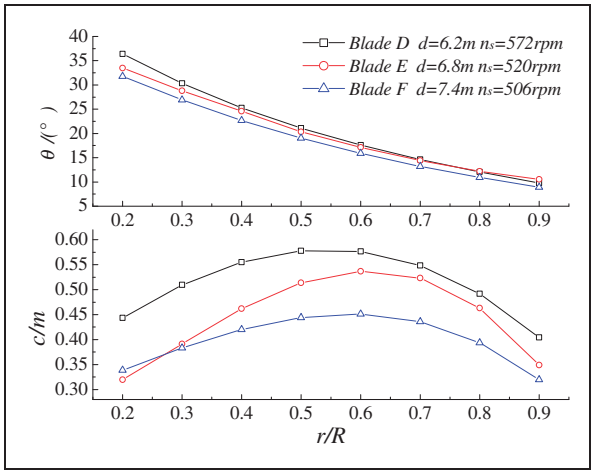

Figure 16. Chord and pitch angle distributions of blades D, E, and F.

with a certain aspect ratio, and larger aspect ratio helps to reduce the induced drag and increase the lift-drag ratio. Consequently, the propeller with high efficiency is seen to favor larger diameter and smaller chord length shown in Figure 16, while the smaller propeller needs higher rotational speed and larger pitch angle to offset the bad effect on propeller efficiency and assure adequate absorbed power. In addition, the blade surface area of large propellers is obvious smaller under the same condition of efficiency, which indicates that the increase of chord length has a greater impact on the surface area of the propeller than the increase of the diameter. Therefore, a reasonable increase in high altitude propeller's diameter can have the advantage of increasing the efficiency and keeping the blade light weight.

It should be noted that the propeller is a kind of slender body which operates like a cantilever beam which will lead to many difficulties of the propeller's structure and manufacture. The force acted on the

whole propeller is integrated by the section thrust, circumferential force and centrifugal force of each blade element, which would generate deformation including extension, torsion and bending, and even structural damage if the propeller is very long and thin.

Influence of the number of blades

The multi-bladed propeller is usually applied for small propellers to absorb the engine power with the increase of wind speed and flight height. In order to analyze the problem better, the diameter of the propeller is determined to be 6.2 m to prevent the chord length of multi-propellers becoming too small and structurally vulnerable.

Pareto-optimal solutions of propellers with 2, 3, and 4 blades are shown in Figure 17. The result shows that the highest efficiency of the multi-bladed propeller is basically equivalent to that of a two-bladed propeller with the same blade area. This is because the optimal multi-bladed propellers, which are featured by smaller chord length shown in Figure 18, have higher aspect ratio to counteract the loss of efficiency caused by blades interference. Meanwhile, increasing the number of blades decreases the tip loss based on the Prandtl's theory, which tends to have a positive impact on propeller efficiency.[26] This indicates that the effect of increasing the number of blades or chord length is almost the same under the same blade area and diameter conditions for the high propeller efficiency in this case. It is important to note that the interference among multiple blades significantly increases with the decrease of blade surface area, so the efficiency of multi-bladed propellers is reduced faster than that of two-bladed propellers.

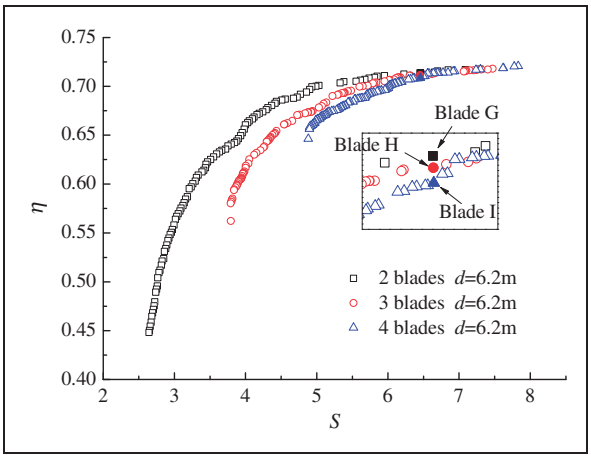

Figure 17. Pareto-optimal solutions of propellers with 2, 3, and 4 blades.

However, the variation of the blade numbers and chord length has a significant impact on the propeller structure. The material density of propeller blades is assumed to be uniform and equal to 5 kg/m^2 in this case. The mass of one blade element, dm, is the product of the blade area, ΔS, and blade density, ρ_b, can be simplified as

$$\mathrm{d}m = \rho_b \Delta S = \rho_b l(x, y)\mathrm{d}r \tag{26}$$

where $l(x, y)$ is the length equation of the blade profile determined in equation (16). Thus, the centrifugal force dF_C of section at position r_0 can be obtained by integrating the centrifugal forces acting on each blade element with respect to r from this blade section radius to the blade tip radius.[27]

$$\mathrm{d}F_C = \int_{r=r_0}^{r_t} (2\pi n_s)^2 r \mathrm{d}m = \int_{r=r_0}^{r_t} (2\pi n_s)^2 r \rho_b l(x, y)\mathrm{d}r \tag{27}$$

The section thrust, dT, and circumferential force, dF_Q, are calculated by the vortex theory. Figure 19 presents the distribution of spanwise force of blades G, H, and I. The aerodynamic force and centrifugal force of multi-bladed propeller blade are much smaller than those of two-bladed propeller and, as a result,

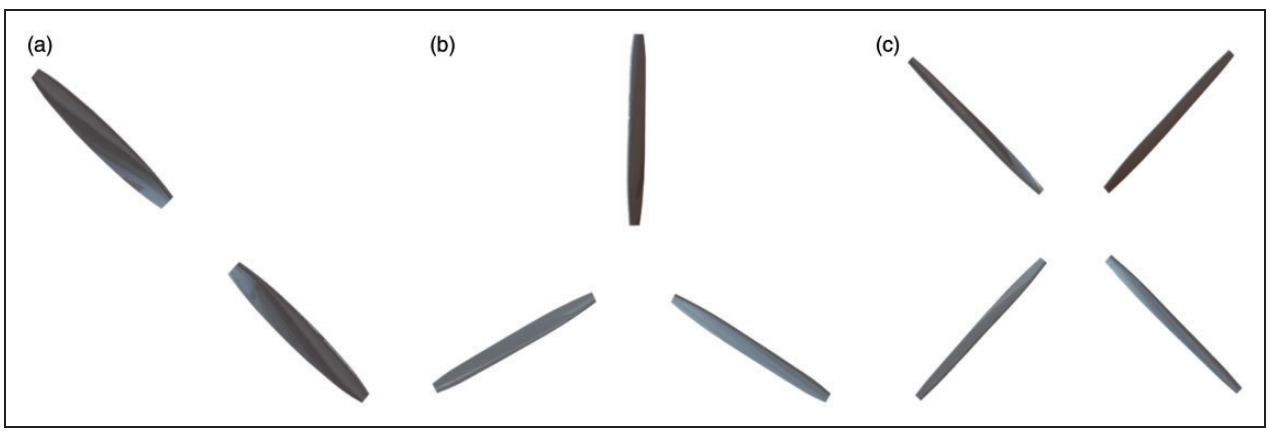

Figure 18. Geometries of propellers G, H, and I: (a) two-bladed propeller; (b) three-bladed propeller; (c) four-bladed propeller.

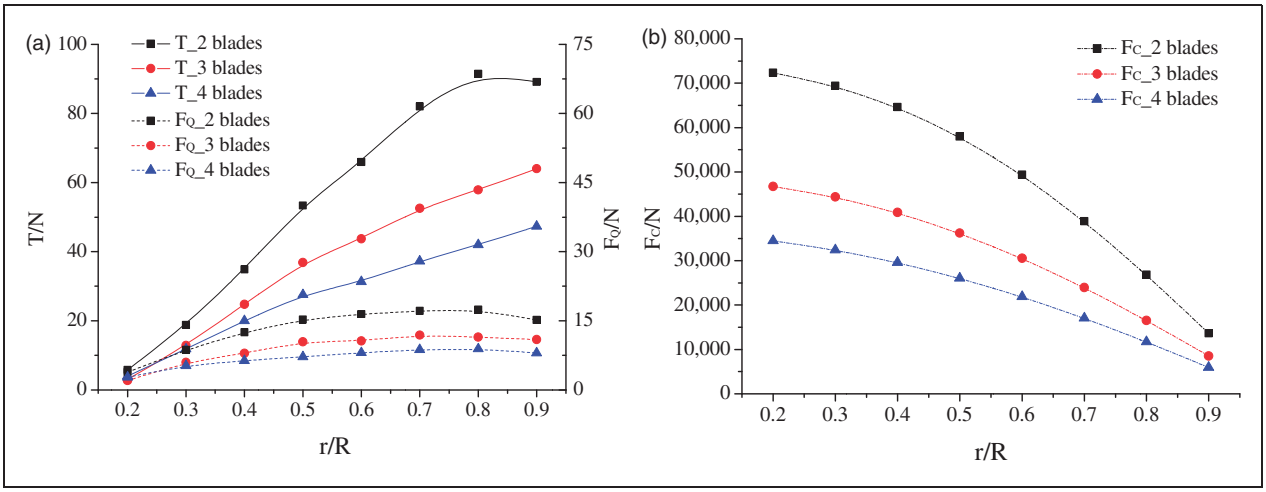

Figure 19. Force distribution of one blade for propellers with 2, 3, and 4 blades: (a) the aerodynamic force distribution; (b) the centrifugal force distribution.

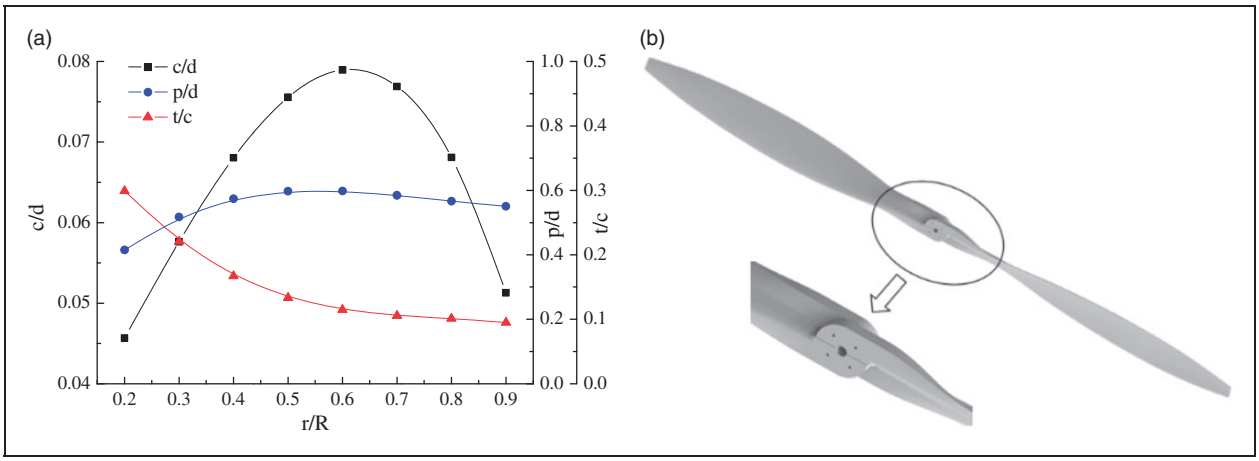

Figure 20. Geometry of the optimal propeller: (a) chord, pitch angle, and thick distribution; (b) shape of the propeller blade and hub.

the multi-bladed propeller is beneficial to structural strength. But just like the situation of increasing the propeller diameter, too many blades for large propellers may lead to a very slender blade which is prone to deformation.

Whereas, in fact, the size and style of the propeller are quite different depending on the different configurations and requirements of the HAA. In some cases, the supporting component of the airship must become longer to avoid scraping the blade tips on the runway or the airship hull as the propeller size increases, and these problems have significant negative effects on a number of other structural and weight issues. Moreover, when the demand of propeller power absorption continues to increase, especially for the small size propeller, the phenomenon discussed above is more notable. Accordingly, multi-bladed propeller could be applied in the high power propulsion design which gives attention to both efficiency and structural strength in such circumstances.

Conversely, instead of simply increasing the motor's power and propeller's surface area, some HAAs choose an optimum power unit design to achieve a better propulsion system by suggesting a rational layout of all devices to avoid a single high-powered propulsion system.[28] Besides, the propeller installation position of some airships is higher than the bottom of the airship hull, and the space for installing is huge enough to use a larger propeller like the use of a stern-mounted propeller for instance.[8] The propeller of HAA in this case, by contrast, could satisfy the propulsion system's power and efficiency requirements by appropriately increasing the propeller diameter.

Results of experiment and calculation

In the practical engineering applications, designers have to make a decision under different working conditions and consider the tradeoff among various

factors to develop a high performance and light weight design. The choice of the optimal propeller in the practical design should be balanced according to the designer's demand with the weight and efficiency. In this project, the important requirement for the HAA propulsion system is to achieve the propeller efficiency of more than 70% at the design point. To this end, the two-bladed propeller with 6.8 m diameter is selected as the final design for the HAA. Figure 20 presents the geometry of the 6.8-meters optimized propeller by pitch ($p = 2\pi r\tan\theta$) ratio, chord ratio and thickness ratio.[26] It is made of composite materials and a mutual inserted hub design.

According to the scaling laws defined in equation (23), the associated parameters of the prototype at design point and model of wind tunnel experiment is introduced in Table 3. Using the test equipment mentioned in the previous section, the wind tunnel experiment and full-scale propeller test were conducted in Shaanxi (altitude 0 km, 34.05°N 108.72°E) and Qinghai (altitude 3.6 km, 35.85°N 99.75°E) provinces in China.

Table 3. The associated parameters of prototype and model.

Parameters	Prototype (design point)	Model (wind tunnel)
Flight altitude (km)	20	0
Air density (kg/m^3)	0.0889	1.2250
Air dynamic viscosity (Pa·s)	1.4216	1.7894
Number of blades	2	2
Diameter (m)	6.8	1
Wind speed (m/s)	20	12.4
Rotational speed (r/min)	510	2154
Reynolds number ($r/R = 0.75$)	625,000	625,000
Advance ratio	0.346	0.346

As shown in Figure 21, the results obtained from the wind tunnel test are in fair agreement with the calculation results of the optimal propeller at different wind velocities. The vortex theory predicts a slightly bigger power coefficient than experimental data, but the maximum efficiency is estimated to be about 8% higher than the test values. This is related to the method's overprediction of the thrust coefficient at high advance ratios. The efficiency of the 1-meter propeller model is about 70.5% at the advance ratio of 0.346, shown in Figure 21(b), and is relatively lower than the calculated result of 75.2%. This indicates that the optimized propeller can satisfy the design requirements of the HAA propulsion system.

The test and computational fluid dynamics (CFD) simulation results[29] of the full-scale propeller are presented in Figure 22. The comparisons are done at two different altitudes and the same wind speed of 10 m/s. It is shown that with the increasing altitude of the test system, the full-scale model has a lower aerodynamic force under the same propeller speed conditions. This is because the dynamic pressure is reduced with an increased altitude as well as the atmospheric density, which leads to the reduction of the lift and drag of each blade element. The mean relative errors of tested thrust and torque compared with CFD simulation values are both less than 10% by computing, and are relatively large when the advance ratio of the propeller is low. It is considered that the main causes of deviation are from two aspects. (1) The testing system is easy to be affected by the vibration of the road and the vehicle. The aerodynamic thrust and torque generated by the propeller are small and can be easily concealed by the vibration interference, especially when the advance ratio is small (propeller operating at low speed). And (2) the flow quality of outdoor

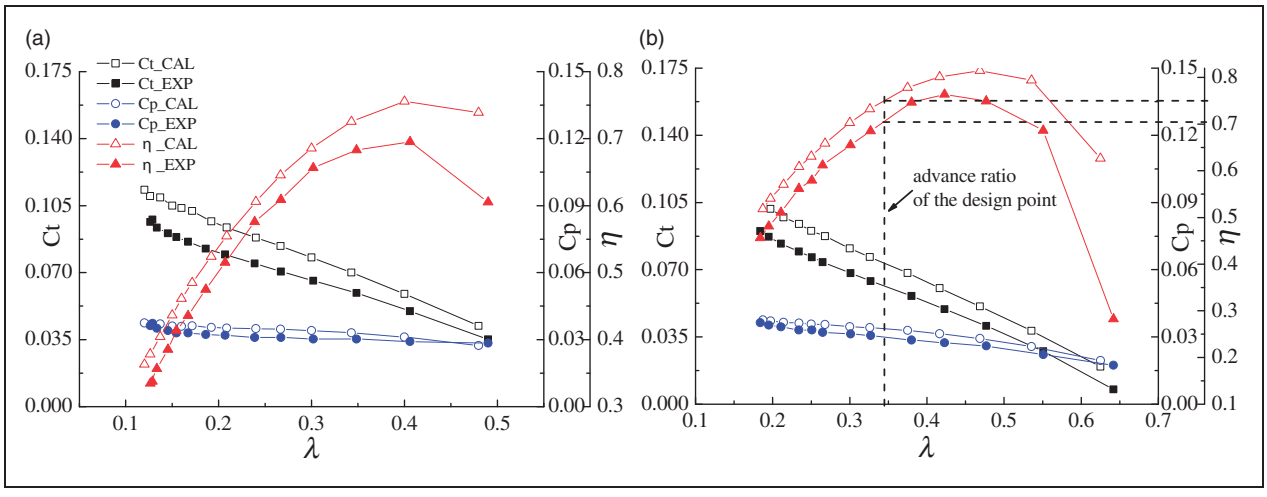

Figure 21. Comparisons of scaled propeller performance between experiment and calculation: (a) performance at wind velocity of 8 m/s; (b) performance at wind velocity of 12.5 m/s.

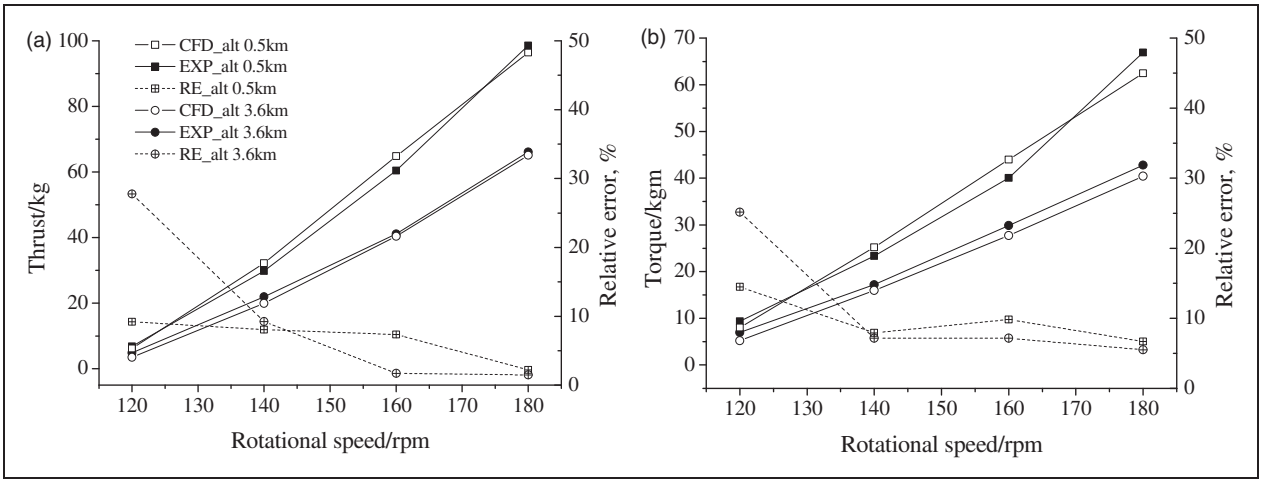

Figure 22. Comparisons of full-scale propeller performance between test and simulation: (a) thrust comparison at different altitudes; (b) torque comparison at different altitudes.

environment including turbulence level, flow stability, flow uniformity, and flow angularity fails to meet the requirements of the wind tunnel. But overall, results obtained from the experiments agree well with those of the numerical simulation, which indicates that there is no large deformation during the operating process of the composite propeller.

Conclusions

In this paper, a multi-objective optimization design of a propeller for HAA is conducted based on the vortex theory and the NSGA-II algorithm. The variation effects of the different design parameters on high altitude propeller's efficiency and weight are discussed in detail on the basis of the Pareto-optimal solutions. The scaled model of the optimized propeller was tested in NF-3 wind tunnel according to the scaling laws, and the full-scale propeller was carried out by the mobile testing system. The following conclusions with guidance on the specific high altitude propeller design are drawn from this study:

(1) The weight of the optimized propeller can be reduced significantly at the cost of a slight decline of efficiency.
(2) Bounded by the same design constraints, appropriately increasing the diameter of high altitude propeller can have the advantage of improving the efficiency and keeping the blade light weight, but it is restricted to motor speed and blade structure.
(3) The optimum efficiency of propellers with different blade numbers is basically the same under the same blade area and diameter conditions, and thus the choice of blade numbers in the design depends on the absorption power and the structural strength.
(4) Results obtained from the two experiments agree well with those of the numerical calculations, and it verifies the validity of the optimization model, and demonstrates that the designed propeller is able to satisfy the requirements of the HAA propulsion system and operate well in the stratosphere.

Acknowledgements

The authors would like to thank the reviewers for their valuable comments and suggestions.

Declaration of Conflicting Interests

The author(s) declared no potential conflicts of interest with respect to the research, authorship, and/or publication of this article.

Funding

The author(s) disclosed receipt of the following financial support for the research, authorship, and/or publication of this article: The research was funded by the National Natural Science Foundation of China (Grant No. 11302177) and the National High Technology Research and Development Program ("863" Program) of China (Grant No. 2012AA051301).

References

1. Moomey ER. *Technical feasibility of loitering lighter-than-air near-space maneuvering vehicles*. Master Degree Thesis, Air Force Institute of Technology, Wright-Patterson AFB, USA, 2005.
2. Jamison L, Sommer GS and Porche III IR. High-altitude airships for the future force army. Rand Arroyo Center, Santa Monica, CA, USA, 2005.
3. Colozza A and Dolce JL. High-altitude, long-endurance airships for coastal surveillance. NASA/TM-2005-213427, 2005.
4. Colozza A and Dolce J. Initial feasibility assessment of a high altitude long endurance airship. NASA/CR-2003-212724, 2003.
5. Lee M, Smith S and Androulakakis S. The high altitude lighter than air airship efforts at the US army space and missile defense command/army forces strategic command. AIAA Paper 2009-2852, 2009.

6. Inamoto Y, Saito K, Shibasaki K, et al. Flight control testing for the development of stratospheric platform airships. AIAA Paper 2003-6799, 2003.
7. Lee YG, Kim DM and Yeom CH. Development of Korean high altitude platform systems. *Int J Wireless Inform Networks* 2006; 13: 31–42.
8. Ilieva G, Páscoa J, Dumas A, et al. A critical review of propulsion concepts for modern airships. *Open Eng* 2012; 2: 189–200.
9. Dumas A, Trancossi M, Madonia M, et al. Multibody advanced airship for transport. SAE Technical Paper 2011-01-2786, 2011.
10. Pancotti A. An overview of advanced concepts for near-space systems. AIAA Paper 2009-4805, 2009.
11. Adkins CN and Liebeck RH. Design of optimum propellers. *J Propul Power* 1994; 10: 676–682.
12. Colozza A. High altitude propeller design and analysis overview. NASA/CR 98-208520, 1998.
13. Monk JS. *A propeller design and analysis capability evaluation for high altitude application*. Master Degree Thesis, University of the Witwatersrand, South Africa, 2011.
14. Morgado J, Abdollahzadeh M, Silvestre MAR, et al. High altitude propeller design and analysis. *Aerosp Sci Technol* 2015; 45: 398–407.
15. Liu PQ, Ma R, Duan ZZ, et al. Experiment study of light-weight, high-efficiency propeller of stratospheric airships in ground wind tunnel. *J Aerosp Power* 2011; 26: 1775–1781.
16. Greer D, Hamory P, Edwards C, et al. Design and predictions for high-altitude (low Reynolds number) aerodynamic flight experiment. *J Aircraft* 2000; 37: 684–689.
17. McCormick BW. *Aerodynamics, aeronautics, and flight mechanics (Vol. 2)*. New York: John Wiley and Sons, 1995.
18. Drela M. XFOIL: An analysis and design system for low Reynolds number airfoils. In: *Low Reynolds number aerodynamics*. Berlin, Heidelberg: Springer, 1989, pp.1–12.
19. Ma R, Zhong BW and Liu PQ. Optimization design study of low-Reynolds-number high-lift airfoils for the high-efficiency propeller of low-dynamic vehicles in stratosphere. *Sci China Technol Sci* 2010; 53: 2792–2807.
20. Coello CC, Lamont GB and Van Veldhuizen DA. *Evolutionary algorithms for solving multi-objective problems*. New York: Springer Science & Business Media, 2007.
21. Bekele EG and Nicklow JW. Multi-objective automatic calibration of SWAT using NSGA-II. *J Hydrology* 2007; 341: 165–176.
22. Nassif N, Kajl S and Sabourin R. Optimization of HVAC control system strategy using two-objective genetic algorithm. *HVAC&R Res* 2005; 11: 459–486.
23. Colozza AJ. APEX 3D propeller test preliminary design. NASA/CR-2002-211866, 2002.
24. Mason Morris LD, Arena A, Gaeta R, et al. Development of a dynamic propulsion test apparatus. AIAA Paper 2014-1311, 2014.
25. Liu PQ, Duan ZZ, Ma LC, et al. Aerodynamics properties and design method of high efficiency-light propeller of stratospheric airships. In: *International conference on remote sensing, environment and transportation engineering (RSETE)*, Nanjing, China, June 2011.
26. Hartman EP and Biermann D. The aerodynamic characteristics of full-scale propellers having 2, 3, and 4 blades of Clark y and RAF 6 airfoil sections. NACA-TR-640, 1938.
27. Glauert H. Airplane propellers. In: *Aerodynamic theory*. Berlin, Heidelberg: Springer, 1935, pp.169–360.
28. Chen S, Song B and Wang H. Exploring optimum power unit of propulsion system for high altitude airship. *Proc IMechE, Part G: J Aerospace Engineering* 2015; 229: 301–311.
29. Xu JH, Song WP, Han ZH, et al. A modified AUSM+-up scheme for simulation of flow around rotary blades. AIAA Paper 2014-1429, 2014.

Appendix

Notation

a	speed of sound
B	number of propeller blades
c	chord length
C_d	drag coefficient
C_l	lift coefficient
C_P	propeller power coefficient, $P/\rho n_s^3 d^5$
C_Q	propeller torque coefficient, $Q/\rho n_s^2 d^5$
C_T	propeller thrust coefficient, $T/\rho n_s^2 d^4$
d	propeller diameter
$d[\,]$	variable at the blade section
D	drag
F	Prandtl's tip loss factor
F_C	centrifugal force
F_Q	circumferential force
H	flight altitude
l	length of blade section profile
L	lift
m	blade mass
Ma	Mach number
Ma_{tip}	blade tip Mach number
n_s	propeller rotational speed
P	propeller adsorbed power
P_p	propeller's required power
Q	propeller torque
r	propeller radial position
r_h	propeller hub radius
r_t	propeller tip radius
R	propeller radius
Re	Reynolds number
S	blade surface area
T	propeller thrust
V	wind velocity
V_E	total relative airspeed
α	angle of attack
α_i	induced angle
β	pitch angle
β_t	blade tip pitch angle
η	propeller efficiency
η_b	efficiency of blade element
γ	drag-lift angle
Γ	circulation about the propeller blade

κ	Goldstein's kappa factor
λ	propeller advance ratio
μ	dynamic viscosity
ν	kinematic viscosity
ω	induced velocity
ω_a	axial component of induced velocity
ω_t	tangential component of induced velocity
φ	advanced angle
ρ	air density
ρ_b	blade density
θ	total down wash angle
$[\,]_m$	variable of propeller model
$[\,]_p$	variable of propeller prototype
$[\,]_r$	ratio of associated variables